Distinguishing nonstandard interaction and Lorentz invariance violation at the Protvino to super-ORCA experiment

Rudra Majhi[1,*], Dinesh Kumar Singha[1,†], Monojit Ghosh[2,‡] and Rukmani Mohanta[1,§]

[1]*School of Physics, University of Hyderabad, Hyderabad 500046, India*
[2]*Center of Excellence for Advanced Materials and Sensing Devices, Ruder Bošković Institute,*
10000 Zagreb, Croatia

As the two phenomena nonstandard interaction (NSI) in neutrino propagation and Lorentz invariance violation (LIV) modify the Hamiltonian of neutrino oscillation in a similar fashion, it is very difficult to distinguish these two effects. The only difference between them lies in the fact that NSI depends on the matter density, whereas LIV is independent of the earth matter effect. Therefore for a fixed baseline experiment, where matter density is constant, the theories describing NSI and LIV are exactly equivalent. However, as the present and future bounds of the NSI and LIV parameters are not equivalent, one can distinguish these two scenarios in the long-baseline neutrino experiments depending on their statistics with respect to the present and future bounds of these parameters. In this paper, we attempt to differentiate between LIV and NSI in the context of DUNE and P2SO, as these two future experiments are believed to be sensitive to the strongest matter effect and will have very large statistics. Taking LIV in the data and NSI in theory, our results show that indeed it is possible to have good discrimination between LIV and NSI. The best separation between LIV and NSI at 3σ C.L. is achieved for the parameter $a_{\mu\mu}$ with P2SO. In this case, the value of the LIV parameter, for which separation is possible, lies within its future bound if one considers the value of NSI parameter to be constrained by the present experiments. Between DUNE and P2SO, the latter has better sensitivity for such discrimination.

I. INTRODUCTION

The Standard Model (SM) of particle physics is quite successful in explaining the interaction of the elementary particles. However, it is well known that SM cannot unravel some of the experimental observations, e.g., tiny neutrino masses and neutrino oscillation. Hence, neutrino oscillation opens up the window for beyond the SM physics. Various neutrino oscillation experiments, like solar-, atmospheric-, reactor-, and accelerator-based ones, have measured the oscillation parameters with great precision within the standard three flavor framework [1]. Thus, the phenomenon of neutrino oscillation also provides a great opportunity to explore several new physics scenarios beyond the standard three flavor framework.

---
[*]rudra.majhi95@gmail.com
[†]dinesh.sin.187@gmail.com
[‡]mghosh@irb.hr
[§]rmsp@uohyd.ac.in

Two of these new physics scenarios are nonstandard interactions (NSI) in neutrino propagation [2–4] and Lorentz invariance violation (LIV) [5], which are studied extensively in neutrino oscillation experiments. In case of nonstandard interactions, the initial and final flavor of the neutrinos can be different due to the interactions of the propagating neutrinos with the earth matter [6]. On the other hand, it has been shown that Lorentz symmetry, which is one of the fundamental symmetries of quantum field theory related to space and time, can be violated in the low energy theories and, hence, can be detected through neutrino oscillation [7]. The effect of both NSI and LIV are well explored in the context of the neutrino oscillation. For studies on NSI, we refer to Refs. [8–43] and, for studies in LIV, we refer to Refs. [44–58]. Although the physics behind NSI and LIV are quite different, the modification in the Hamiltonian of neutrino propagation due to NSI and LIV are very similar. The only difference lies in the fact that the effect of NSI is more prominent in the presence of matter, whereas LIV is not affected by the matter density. Therefore, in neutrino oscillation experiments, it is arduous to distinguish the effects of NSI and LIV. Recently, an effort was made to distinguish these two phenomena in the context of atmospheric neutrino experiment ICAL [59] where one can have different earth matter densities over

various baseline lengths. For long-baseline experiments, where the matter density is constant, the theories of NSI and LIV are exactly equivalent. However, as the present and future bounds of the NSI and LIV parameters are not in the equal footing, it is possible to discriminate these two scenarios in the long-baseline experiments. Depending on the value of matter density and statistics, one can have a significant difference between the two theories. In this paper, for the first time we study the possibility of distinguishing NSI and LIV at the following long-baseline neutrino experiments: Deep Underground Neutrino Experiment (DUNE) [60] in Fermilab with a baseline of 1300 km and Protvino to Super-ORCA (P2SO) [61] at KM3NeT [62] facility with a baseline of 2595 km. These two future experiments will have the most notable matter effect and higher statistics. In this work, our strategy will be to take LIV in the simulated data and NSI in theory and study the capability of these two future neutrino oscillation experiments to distinguish LIV from NSI, using current and future bounds of the NSI parameters. As future experiments will be able to put stronger bounds on the NSI parameters, we expect a higher distinguishability of LIV from NSI when we use the future bounds of the NSI parameters in the analysis.

The paper is organized as follows. In the next section, we present the theoretical background of NSI and LIV and illustrate how the Hamiltonian of the neutrino oscillation gets modified by the presence of NSI and LIV. Then we discuss the specification of the experiments and the details of numerical analysis that has been used in our calculation. After that, we will briefly outline the present and future possible bounds on the NSI and LIV parameters. Then we will estimate the sensitivity of DUNE and P2SO to discriminate between the two phenomena with respect to their present and future possible bounds. Finally, we summarize our results and conclude.

II. THEORETICAL BACKGROUND

The neutral current nonstandard interaction between the propagating neutrinos and fermions in the earth matter can be written in terms of the interaction Lagrangian [4]

$$\mathcal{L}_{\text{NSI}} = -2\sqrt{2}G_F\epsilon_{\alpha\beta}^{fC}(\bar{\nu}_\alpha\gamma^\mu P_L\nu_\beta)(\bar{f}\gamma_\mu P_C f), \quad (1)$$

where G_F represents the Fermi constant, $\epsilon_{\alpha\beta}^{fC}$ are the NSI parameters characterizing the strength of nonstandard interactions with α, $\beta = e, \mu, \tau$, the fermion fields are represented by $f = e, u, d$, and P_C with $C = L, R$ stand for the left and right chiral projection operators. For the neutrino propagation in the earth, the relevant combinations of the NSI parameters are expressed as

$$\epsilon_{\alpha\beta} = \sum_{f=e,u,d}\epsilon_{\alpha\beta}\frac{N_f}{N_e} = \sum_{f=e,u,d}(\epsilon_{\alpha\beta}^{fL} + \epsilon_{\alpha\beta}^{fR})\frac{N_f}{N_e}, \quad (2)$$

where N_f represents the number density of f fermion. For the Earth matter, which is considered as neutral and isoscalar, one can have $N_n \simeq N_p = N_e$, which essentially implies $N_u \simeq N_d \simeq 3N_e$. Hence, one can write the NSI parameters as

$$\epsilon_{\alpha\beta} \simeq \epsilon_{\alpha\beta}^e + 3\epsilon_{\alpha\beta}^u + 3\epsilon_{\alpha\beta}^d. \quad (3)$$

The effective Lagrangian density describing LIV in neutrino interactions can be written as [50,63,64]

$$\mathcal{L}_{\text{LIV}} = -\frac{1}{2}[p_{\alpha\beta}^\mu\bar{\nu}_\alpha\gamma_\mu\nu_\beta + q_{\alpha\beta}^\mu\bar{\nu}_\alpha\gamma_5\gamma_\mu\nu_\beta \\ - ir_{\alpha\beta}^{\mu\nu}\bar{\nu}_\alpha\gamma_\mu\partial_\nu\nu_\beta - is_{\alpha\beta}^{\mu\nu}\bar{\nu}_\alpha\gamma_5\gamma_\mu\partial_\nu\nu_\beta], \quad (4)$$

where $p_{\alpha\beta}^\mu$, $q_{\alpha\beta}^\mu$, $r_{\alpha\beta}^{\mu\nu}$, and $s_{\alpha\beta}^{\mu\nu}$ are the Lorentz violating parameters in the flavor basis. As only the left-handed neutrinos exist in nature, the LIV parameters can be parametrized by the following observable quantities, which are combinations of $p_{\alpha\beta}^\mu$, $q_{\alpha\beta}^\mu$, $r_{\alpha\beta}^{\mu\nu}$, and $s_{\alpha\beta}^{\mu\nu}$:

$$(a_L)_{\alpha\beta}^\mu = (p+q)_{\alpha\beta}^\mu, \quad \text{and} \quad (c_L)_{\alpha\beta}^{\mu\nu} = (r+s)_{\alpha\beta}^{\mu\nu}, \quad (5)$$

where $(a_L)_{\alpha\beta}^\mu$ are related to CPT violating neutrino interactions and $(c_L)_{\alpha\beta}^{\mu\nu}$ are associated with CPT even, Lorentz violating interactions. For long baseline experiments the effective Hamiltonian in the presence of both NSI and LIV can be written as

$$H = H_{\text{vac}} + H_{\text{mat}} + H_{\text{NSI}} + H_{\text{LIV}}, \quad (6)$$

where H_{vac} and H_{mat} represent the vacuum and standard matter Hamiltonian whereas H_{NSI} and H_{LIV} represent the NSI and LIV Hamiltonian. The different components of the Hamiltonian can be expressed as

$$H_{\text{vac}} = \frac{1}{2E}U\begin{pmatrix} m_1^2 & 0 & 0 \\ 0 & m_2^2 & 0 \\ 0 & 0 & m_3^2 \end{pmatrix}U^\dagger, \quad (7)$$

$$H_{\text{mat}} = \sqrt{2}G_FN_e\begin{pmatrix} 1 & 0 & 0 \\ 0 & 0 & 0 \\ 0 & 0 & 0 \end{pmatrix}, \quad (8)$$

$$H_{\text{NSI}} = \sqrt{2}G_FN_e\begin{pmatrix} \epsilon_{ee} & \epsilon_{e\mu} & \epsilon_{e\tau} \\ \epsilon_{e\mu}^* & \epsilon_{\mu\mu} & \epsilon_{\mu\tau} \\ \epsilon_{e\tau}^* & \epsilon_{\mu\tau}^* & \epsilon_{\tau\tau} \end{pmatrix}, \quad \text{and} \quad (9)$$

$$H_{\text{LIV}} = \begin{pmatrix} a_{ee} & a_{e\mu} & a_{e\tau} \\ a_{e\mu}^* & a_{\mu\mu} & a_{\mu\tau} \\ a_{e\tau}^* & a_{\mu\tau}^* & a_{\tau\tau} \end{pmatrix} - \frac{4}{3}E\begin{pmatrix} c_{ee} & c_{e\mu} & c_{e\tau} \\ c_{e\mu}^* & c_{\mu\mu} & c_{\mu\tau} \\ c_{e\tau}^* & c_{\mu\tau}^* & c_{\tau\tau} \end{pmatrix}, \quad (10)$$

where the parameters m_1, m_2, and m_3 represent the masses of the neutrinos, which enter into the neutrino oscillation probabilities as $\Delta m_{21}^2 = m_2^2 - m_1^2$ and $\Delta m_{31}^2 = m_3^2 - m_1^2$. The Pontecorvo–Maki–Nakagawa–Sakata (PMNS) matrix U contains three mixing angles θ_{12}, θ_{13}, and θ_{23} and one Dirac type phase δ_{CP}. If we neglect the contribution from the *CPT* conserving LIV parameters, then the effect of NSI is analogous to LIV as can be seen in Eq. (10). The only difference is that NSI effects explicitly depend on the matter density while LIV is independent of matter. From the above equations, one can obtain the correlation between the NSI and LIV parameters as

$$a_{\alpha\beta} = \sqrt{2} G_F N_e \epsilon_{\alpha\beta}. \qquad (11)$$

The matter potential part can be written as

$$\sqrt{2} G_F N_e \simeq 7.5 X_e \frac{\rho}{10^{14} \ (\text{g/cm}^3)} \ \text{eV}, \qquad (12)$$

where X_e is the relative electron number density and for a neutral medium $X_e = 0.5$. The matter density is given by ρ in the units of g/cm^3. From the above two equations, we obtain

$$a_{\alpha\beta} = 3.75 \times \frac{\rho}{(\text{g/cm}^3)} \times 10^{-23} \epsilon_{\alpha\beta} \ \text{GeV}. \qquad (13)$$

For long-baseline experiments ρ is approximately constant. Therefore, we understand that, for an upper bound of the NSI parameter with the value $\epsilon_{\alpha\beta}$, it can be distinguished from LIV only if the LIV parameters are larger than $3.75 \times \rho \times 10^{-23} \epsilon_{\alpha\beta}$ GeV. For DUNE, the value of ρ is 2.848 g/cm^3 and for P2SO the value is 2.95 g/cm^3. In the next section, we will see that the present and future bounds of the NSI and LIV parameters are not connected by the above relation and, therefore, it is possible to separate these two scenarios in DUNE and P2SO with respect to their current/future bounds. In this case, the significance of the separation will depend on the statistics of both the experiments.

III. EXPERIMENTAL SETUP AND SIMULATION DETAILS

We have used the GLoBES [65,66] software package to simulate DUNE and P2SO. We have further used additional plugins of GLoBES to implement NSI [67] and modified the NSI probability engine accordingly to incorporate LIV.

For simulating the long-baseline experiment P2SO, we use the same configuration as used in Ref. [68]. The Protvino accelerator houses a 1.5 km-diameter U-70 synchrotron that generates a 450 KW beam corresponding to 4×10^{20} POT annually for P2SO configuration. The Super-ORCA detector located at a distance of 2595 km from Protvino, which is ten times more dense than the

TABLE I. The values of oscillation parameters that we considered in our analysis. Standard oscillation parameters considered from [1] with their corresponding 1σ errors.

Parameters	True values $\pm 1\sigma$
$\sin^2\theta_{12}$	$0.304^{+0.013}_{-0.012}$
$\sin^2\theta_{13}$	$0.0222^{+0.00068}_{-0.00062}$
$\sin^2\theta_{23}$	$0.573^{+0.018}_{-0.023}$
$\delta_{\text{CP}}[°]$	195^{+52}_{-25}
Δm_{21}^2 [10^{-5} eV^2]	$7.42^{+0.21}_{-0.20}$
Δm_{31}^2 [10^{-3} eV^2]	$2.515^{+0.028}_{-0.028}$

ORCA detector, will be used in the P2SO experiment. Three years in neutrino mode and three years in antineutrino mode made up to a total runtime of six years for P2SO. In P2SO, the energy window for event calculation ranges from 0.2 to 10 GeV.

For DUNE, we have used the official GLoBES files corresponding to the technical design report [69]. At a distance of 1300 km from the neutrino source at Fermilab, a 40 kt liquid argon time-projection chamber detector with a power of 1.2 MW is placed. The total runtime for DUNE is seven years comprising of 3.5 years in neutrino mode and 3.5 years in antineutrino mode, corresponding to 1.1×10^{21} POT annually.

For the estimation of the sensitivity, we use the Poisson log-likelihood and assume that it is χ^2 distributed:

$$\chi_{\text{stat}}^2 = 2 \sum_{i=1}^{n} \left[N_i^{\text{test}} - N_i^{\text{true}} - N_i^{\text{true}} \log\left(\frac{N_i^{\text{test}}}{N_i^{\text{true}}}\right) \right], \qquad (14)$$

where N^{test} and N^{true} are the number of events in the test and true spectra, respectively, and i is the number of energy bins. The systematic is incorporated by the method of pull [70,71]. The best-fit values of the standard oscillation parameters and their 1σ ranges are adopted from NuFIT [1], which are listed in Table I. The NSI and LIV parameters and their current and future bounds are presented in Tables III and IV, and will be discussed in detail in the next section. Utilizing the built-in minimizer in GLoBES and incorporating the priors corresponding to

TABLE II. The values of systematic errors that we considered in our analysis: "norm" stands for normalization error, "Sg" stands for signal, and "Bg" stands for background.

Systematics	P2SO	DUNE
Sg-norm ν_e	5%	2%
Sg-norm ν_μ	5%	5%
Bg-norm	12%	5% to 20%
Sg-shape	11%	...
Bg-shape	4% to 11%	...

their 1σ uncertainties, we marginalized over all the relevant parameters in our analysis. The NSI parameters are varied and marginalized according to Table III. For δ_{CP}, we have not considered any prior initially and allowed it to vary freely. For systematic uncertainties, we have considered the overall normalization and shape errors corresponding to signal and background. We list the values of systematic errors for P2SO and DUNE in Table II. It should be noted that the DUNE GLoBES file contains no shape error. We show all our results for the normal hierarchy of the neutrino masses, i.e., for $\Delta m_{31}^2 > 0$.

IV. BOUNDS ON NSI AND LIV PARAMETERS

In Table III, we have listed the current and future bounds on the NSI parameters at 90% confidence limit (C.L.) The upper bounds on the NSI parameters are calculated in many studies [2–4,41,42,72,73]. The bounds on the NSI parameters can be either model dependent or model independent. For our study, we consider only the model independent bounds. The strongest current bounds for $\epsilon_{e\mu}$, ϵ_{ee}, and $\epsilon_{\mu\mu}$ are calculated in Ref. [41] by considering the global data. For the parameters $\epsilon_{e\tau}$ and $\epsilon_{\mu\tau}$, the current strongest bounds come from the Super-Kamiokande data [74] whereas for $\varepsilon_{\tau\tau}$ a stronger bound has been obtained in the KamLAND+SNO/ Super-K data [72]. In future, the strongest bounds for the parameters $\epsilon_{e\mu}$, $\epsilon_{e\tau}$, and ϵ_{ee} are expected to come from DUNE [33] and regarding parameters $\epsilon_{\mu\tau}$ and $\epsilon_{\tau\tau}$ the best future bounds will come from PINGU [75]. For the parameter $\epsilon_{\mu\mu}$, the stringent future bound is expected to come from the neutrino factory experiments [72]. From Table III, we understand that future experiments will be able to put an order of magnitude better constraints on the NSI parameters, compared to current bounds except $\epsilon_{\mu\mu}$.

In Table IV, we have shown the bounds on LIV parameters from different neutrino experiments at 90% C.L. Currently the Super-Kamiokande experiment can give strong bounds on $a_{e\mu}$, $a_{e\tau}$, and $a_{\mu\tau}$ [48]. The current best limits on LIV parameters a_{ee}, $a_{\mu\mu}$, and $a_{\tau\tau}$ are obtained from combination of NOνA and T2K [50]. In future, very constraint limits on all parameters except $a_{\mu\tau}$ and $a_{\tau\tau}$ are expected from the combination of DUNE and P2O as discussed in Ref. [46]. ICAL experiment can put the

TABLE III. Current and future bounds on NSI parameters at 90% C.L.

| | NSI | |
Parameter	Current bound	Future bound
$\epsilon_{e\mu}$	<0.3 [41]	$[-0.036, +0.034]$ [33]
$\epsilon_{e\tau}$	$[-0.19, 0.13]$ [74]	$[-0.031, +0.031]$ [33]
ϵ_{ee}	<4 [41]	$[-0.206, +0.278]$ [33]
$\epsilon_{\mu\mu}$	<0.068 [41]	<0.0307 [72]
$\epsilon_{\mu\tau}$	<0.011 [74]	$[-0.0043, 0.0047]$ [75]
$\epsilon_{\tau\tau}$	$[-4.4, 3.9]$ [72]	$[-0.03, 0.017]$ [75]

TABLE IV. Current and future bounds on LIV parameters in the units of 10^{-23} GeV at 90% C.L.

| | LIV | |
Parameter	Current bound	Future bound
$a_{e\mu}$	<2.4 [48]	<0.39 [46]
$a_{e\tau}$	<4.24 [48]	<0.55 [46]
a_{ee}	$[-49.5, +26.5]$ [50]	$[-1.95, 2.46]$ [46]
$a_{\mu\mu}$	$[-10, 11]$ [50]	$[-1.24, 1.39]$ [46]
$a_{\mu\tau}$	<0.79 [48]	$[-0.19, 0.18]$ [47]
$a_{\tau\tau}$	$[-9.8, 8.2]$ [50]	$\cdots$

strongest bound on $a_{\mu\tau}$ as discussed in Ref. [47]. To the best of our knowledge, the future model independent bound on the parameter $a_{\tau\tau}$ is yet to be determined. From Table IV, we understand that future experiments will be able to put an order of magnitude better bounds on the LIV parameters, compared to current bounds except $a_{\mu\tau}$.

Note that the bounds on different NSI and LIV parameters are calculated with different initial conditions. For example, with different values of oscillation parameters, inclusion of a different number of parameters at a time, etc. Therefore, it would be improper to treat all the bounds at the same footing and it only gives us an order of magnitude estimation.

From Tables III and IV, we see that the present/future bounds of the NSI and LIV parameters do not obey the equivalence relation as given in Eq. (13). For example, the bound on $\epsilon_{\mu\mu}$, is one order of magnitude stronger than the bound on $a_{\mu\mu}$. This provides the opportunity to separate these two phenomena in the fixed density experiments with respect to their bounds, which we will see in the next section.

V. DISCRIMINATION AT PROBABILITY LEVELS

In this section, we will try to distinguish between NSI and LIV effects at the probability level with the long baseline experiments. The neutrino oscillation probabilities are modified in the presence of NSI and LIV. The probability of finding a neutrino ν_β from a α type neutrino ν_α, after the propagation of distance L, is

$$P_{\alpha\beta} = |\langle\nu_\beta|\nu_\alpha(L)\rangle|^2 = |\langle\nu_\beta|e^{-iHL}|\nu_\alpha\rangle|^2, \quad (15)$$

where H is the effective Hamiltonian in presence of LIV or NSI effects, which we discussed earlier. Exact expression for oscillation probability can be found in Refs. [8,11,12,20,25,76–81].

In these calculations, it is shown that the NSI as well as LIV parameters corresponding to $e\mu$, $e\tau$, and ee sectors have leading order contribution to the appearance probability, i.e., $\nu_\mu \to \nu_e$, while the NSI and LIV parameters involving $\mu\mu$, $\mu\tau$, and $\tau\tau$ sectors affect significantly to the survival probability $\nu_\mu \to \nu_\mu$. Therefore, while discussing the separation between NSI and LIV for $e\mu$, $e\tau$, and
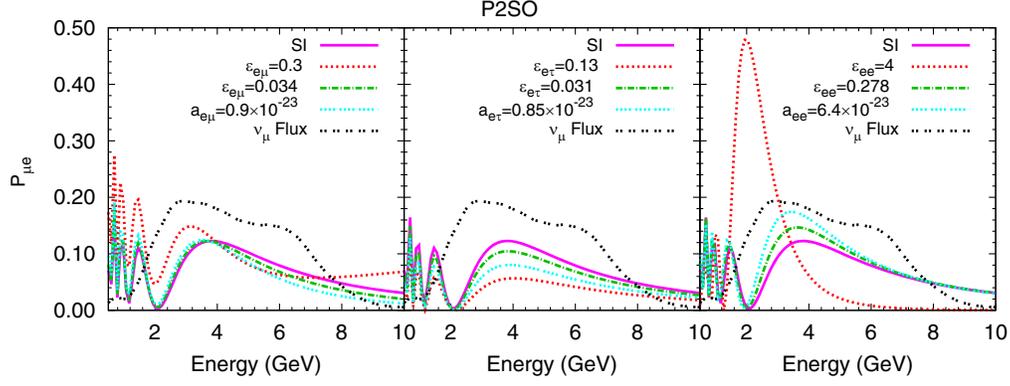
FIG. 1.   Appearance probability as a function of neutrino energy for the P2SO experiment in presence of $(\epsilon_{e\mu}, a_{e\mu})$, $(\epsilon_{e\tau}, a_{e\tau})$, and (ϵ_{ee}, a_{ee}).

ee ($\mu\mu$, $\mu\tau$, and $\tau\tau$) sectors, we will use appearance (disappearance) probability only. In our analysis, we have considered one parameter at a time for each NSI and LIV scenario. Therefore, in our study, we have six independent LIV parameters and six independent NSI parameters. Note that if we do not consider one parameter at a time and rather consider all the parameters at the same time, then number of independent parameters in each LIV and NSI cases would be five. This is because, when one considers all the parameters at the same time, then one can always subtract a matrix proportional to the identity without changing the oscillation probabilities, which leaves only two of the diagonal parameters to be independent.

First, let us discuss the separation between NSI and LIV effects corresponding to the parameters sensitive to the appearance channel. Figure 1 shows the oscillation probability for the ν_e appearance channel as a function of neutrino energy for the P2SO experiment. The left/middle/right panel corresponds to the parameter $e\mu/e\tau/ee$. In each panel, the standard three flavor case (SI) is represented by the solid magenta curve and black dashed curve represents muon flux of P2SO in arbitrary unit. Therefore, the energy region covered by the black curve shows the region to which the P2SO experiment is sensitive. In these panels, the red (green) dashed curve shows the probability including NSI to SI with the value of the NSI parameters corresponding to their current (future) upper bounds as given Table III. For the LIV parameter, we choose a value (cyan) for which a 3σ separation between LIV and NSI is obtained for P2SO, considering the constraints on the NSI parameters from the future experiments as given in Table V. The first thing we observe from these panels is that the first oscillation maxima of P2SO is within the corresponding flux envelope in a standard case as well as in NSI and LIV scenarios. We also note that in all the three panels, around the first oscillation maximum, the cyan curve is always sandwiched between the magenta and red curves but it is mostly outside the region between the magenta and green curves. Or in other words, the difference between SI and NSI is higher (lower) as compared to the difference between SI and LIV for the case of present (future) bound of the NSI

parameters. Therefore, it will be very easy to match the probability of LIV with the NSI probability, i.e., the possibility of a degeneracy between NSI and LIV will be more when the NSI parameters are varied within their current upper bounds, compared to their future bounds. This in turn leads to the fact that the distinction between NSI and LIV would be higher, when we consider the future bounds of NSI parameters compared to their current bounds for a given value of LIV parameter. Among these three parameters, we expect the separation between NSI and LIV to be very weak for ee, if we consider the current bound of the NSI parameter.

Now let us discuss the separation between NSI and LIV corresponding to the parameters, that are sensitive to the disappearance channel, as shown in Fig. 2. The plots in the lower panel are same as Fig. 1 but for the disappearance channel and for the parameters $\mu\mu$ (left panel), $\mu\tau$ (middle panel), and $\tau\tau$ (right panel). We have followed the same philosophy as the appearance channel for choosing the values of NSI and LIV parameters, i.e., red (green) curve shows the probability including NSI to SI with the values of the NSI parameters corresponding to their current (future) upper bounds. The cyan curve is for the LIV parameter and we choose its value such that a 3σ separation between LIV and NSI is obtained for P2SO considering the future bounds of the NSI parameters. As it is difficult to visualize different probabilities at the first minimum, in the upper

TABLE V.   Values of LIV parameters in the units of 10^{-23} GeV for which a 3σ separation with NSI is possible for present (future) bounds on the NSI parameters.

	LIV Parameters	
Parameter	P2SO	DUNE
$a_{e\mu}$	3.7 (0.9)	3.7 (0.95)
$a_{e\tau}$	1.9 (0.85)	2 (1.5)
a_{ee}	$-(6.4)$	$-(7.7)$
$a_{\mu\mu}$	1.3 (0.85)	3.2 (2.8)
$a_{\mu\tau}$	0.2 (0.14)	0.44 (0.38)
$a_{\tau\tau}$	$-(0.7)$	$-(2.65)$
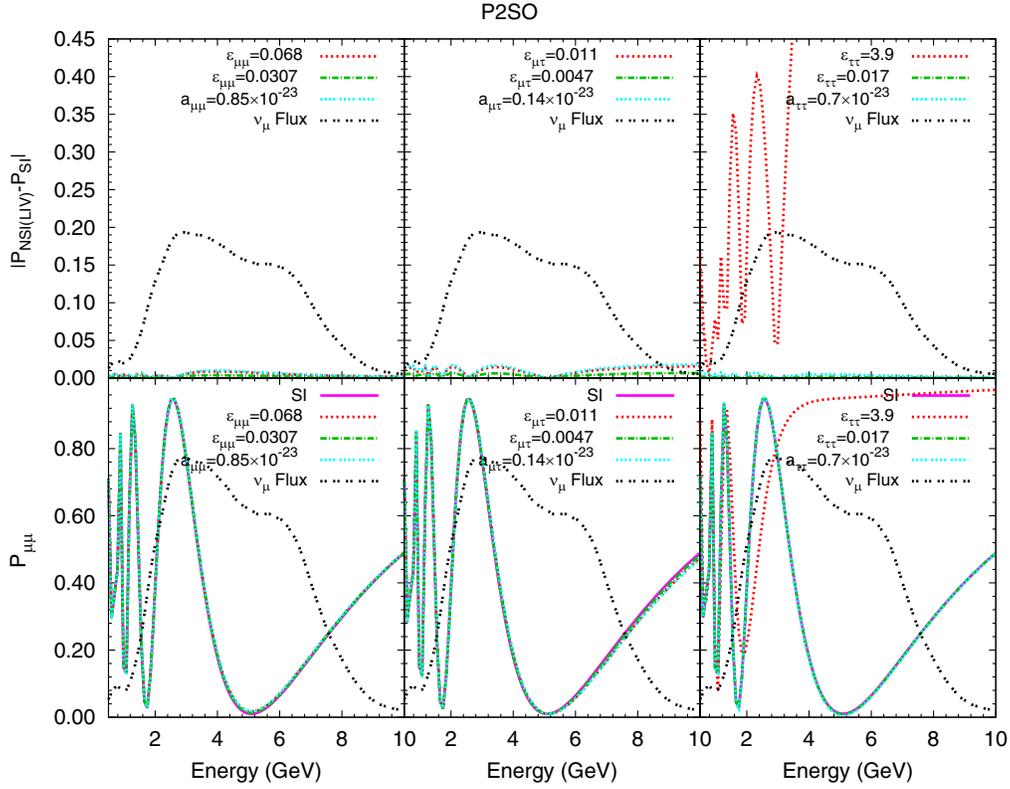
FIG. 2. Survival probability as a function of neutrino energy for P2SO experiment in presence of $(\epsilon_{\mu\mu}, a_{\mu\mu})$, $(\epsilon_{\mu\tau}, a_{\mu\tau})$, and $(\epsilon_{\tau\tau}, a_{\tau\tau})$.

panel, we have plotted the probability difference between SI to NSI and SI to LIV. From these plots, we also see that the difference between SI and NSI is either higher or equal to SI and LIV, when we consider the values of NSI parameters corresponding to their current bounds and it is lower when we consider the values of NSI corresponding to their future bounds. Therefore, as in appearance channel, we expect to have better separation between LIV and NSI for future bounds of NSI compared to their current bounds. Among these three parameters, the separation for $\tau\tau$ is found to be very weak if we consider the current bounds of the NSI parameters.

For DUNE, we have checked that the behavior of the probability plots are very similar to that of P2SO, and therefore we do not present the figures for DUNE.

VI. ELIMINATION OF DEGENERACY

In order to discriminate the degeneracy between NSI and LIV phenomena, we have calculated $\chi^2_{\min}$ considering LIV exists in nature and NSI as the test hypothesis, i.e.,

$$\chi^2 \sim N^{\text{test}}(\epsilon_{\alpha\beta}^{\text{test}} \neq 0, a_{\alpha\beta}^{\text{test}} = 0) - N^{\text{true}}(\epsilon_{\alpha\beta}^{\text{true}} = 0, a_{\alpha\beta}^{\text{true}} \neq 0).$$

We have obtained sensitivities for two cases of the NSI parameters, i.e., minimizing the NSI parameters either within their current bounds or their future bounds. In Fig. 3, we have shown the sensitivities for the parameters

that appear in the appearance channel probabilities, i.e., $e\mu$, $e\tau$, and ee, and, in Fig. 4, we have presented the sensitivities for the parameters appearing in the disappearance channel probabilities, i.e., $\mu\mu$, $\mu\tau$, and $\tau\tau$. In each figure, the plots in the upper panel are for DUNE and in the lower panel are for P2SO. In each panel, the blue curve represents the sensitivity for the current range of the NSI parameters and the red curve represents the sensitivity for the future bounds of the NSI parameters. The black horizontal lines correspond to $\Delta\chi^2 = 4$ and 9, represent the benchmark sensitivities of 2σ and 3σ, respectively.

The panels in Figs. 3 and 4 can be interpreted in the following way. In these panels, a nonzero value of the $\Delta\chi^2$ signifies the sensitivity to discriminate LIV from NSI. On the other hand, the values of $a_{\alpha\beta}$ for which $\Delta\chi^2 = 0$, one cannot distinguish LIV from NSI at all. The values of $a_{\alpha\beta}$, for which $\Delta\chi^2$ is greater than 9, it is possible to separate LIV from NSI at 3σ C.L. From the figures, we see that in general the separation between LIV and NSI is better if we consider future bounds of the NSI parameters, compared to the present limits. This improvement is more in $e\mu$ and $e\tau$ sectors compared to the $\mu\mu$ and $\mu\tau$ sectors. For the parameters ee and $\tau\tau$, it is impossible to discriminate LIV from NSI, if we consider the current ranges of the NSI parameters. Between the experiments DUNE and P2SO, better separation between NSI and LIV is obtained for P2SO except for the $e\mu$ sector.
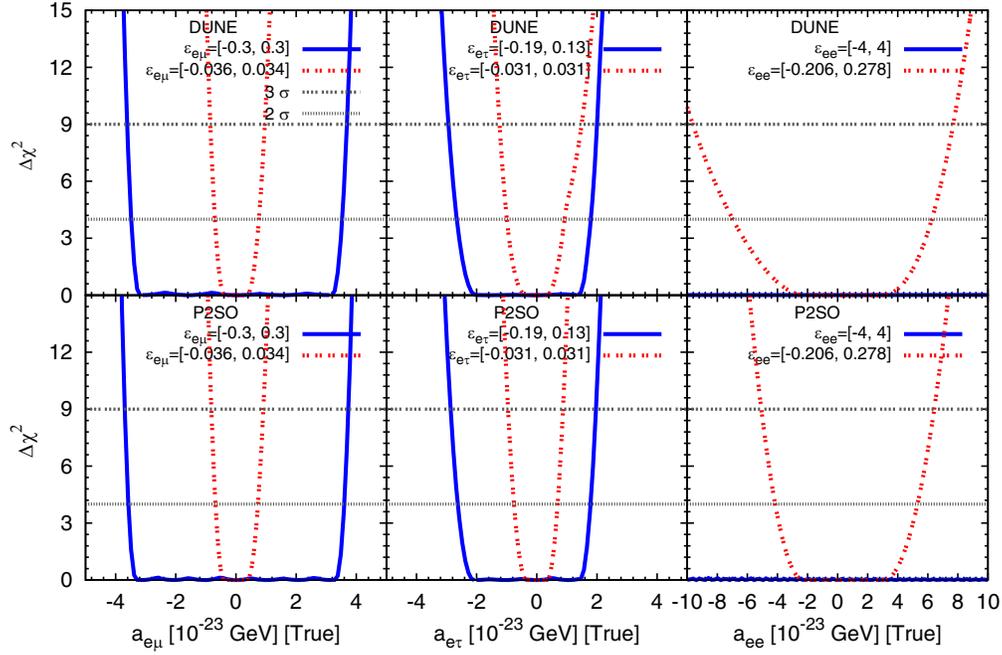
FIG. 3. $\Delta\chi^2$ as a function of true LIV parameters $a_{e\mu}$, $a_{e\tau}$, and a_{ee} for P2SO and DUNE experiments.
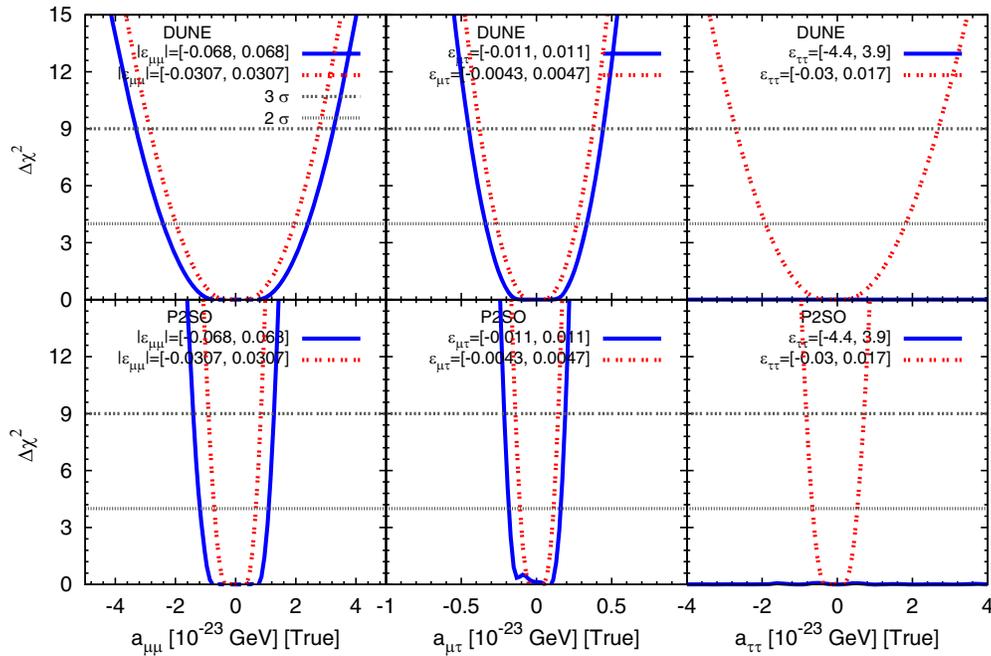
FIG. 4. $\Delta\chi^2$ as a function of true LIV parameters $a_{\mu\mu}$, $a_{\mu\tau}$, and $a_{\tau\tau}$ for P2SO and DUNE experiments.

In Table V, we have listed the values of LIV parameters for which a 3σ separation with NSI is possible.

From the table, we understand that the better discrimination between LIV and NSI is possible for the P2SO experiment. Regarding a 3σ discrimination between LIV

and NSI, from Tables V and IV, we can infer the following in the context of P2SO:

(1) The best discrimination between LIV and NSI is possible for the $\mu\mu$ sector. For this sector, it is possible to have a separation for the value of LIV
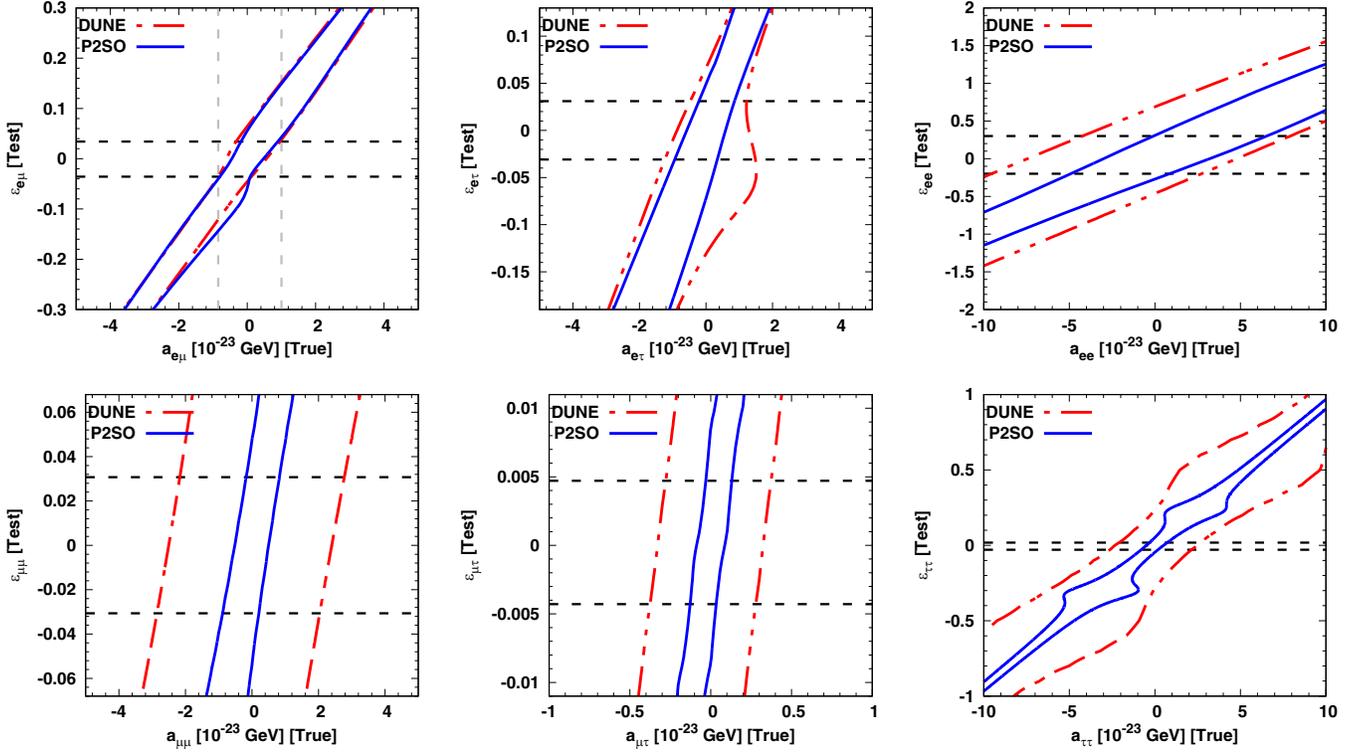
FIG. 5. 3σ contours in $a_{\alpha\beta}$[True]-$\epsilon_{\alpha\beta}$[Test] plane. Horizontal lines represent the future bounds of corresponding NSI parameters $\epsilon_{\alpha\beta}$.

parameter within its future bound, if one considers the value of NSI parameter to be constrained by the present experiments.

(2) For the sectors $e\tau$ and $\mu\tau$, the discrimination is possible for the values of LIV parameters within their present bounds but outside their future bounds, if one considers the values of NSI parameters to be constrained by the present experiments.

(3) For $e\mu$ sector, discrimination occurs for the values of LIV parameter within its present bound but outside its future bound, if one considers the value of the NSI parameter to be constrained by the future experiments. For values of NSI parameter inside the present bound, the values of LIV parameter for which discrimination is possible lie outside the present bound.

(4) Regarding the sectors ee and $\tau\tau$ the sensitivity is worst. For these two cases, the separation is possible for the values of LIV parameters within their present bounds and outside the future bound (for ee), if one considers the values of NSI parameters to be constrained by the future experiments. However, no separation is possible if one considers the NSI parameters to be constrained by the present experiments.

To understand the results in a better way, in Fig. 5, we examined the same situation in a different way. This figure depicts the contours when we consider LIV in true and test this theory against the NSI hypothesis using its future range at 3σ C.L. The red and blue contours are for DUNE and

P2SO, respectively. The horizontal black dashed lines represent the future limits of NSI parameters. The top row is for $e\mu$, $e\tau$, and ee components and the bottom row is for $\mu\mu$, $\mu\tau$, and $\tau\tau$ components.

The area inside the contours represent the values of the LIV parameters that cannot be distinguished from the NSI parameters at the 3σ level. The region outside the contours allows us to discriminate NSI from LIV at the same or higher confidence level. From these panels, we can also see that, in general, the sensitivity is higher for P2SO than DUNE except the $e\mu$ sector. To have a clear understanding of the values of LIV parameters for which we can separate them from NSI, we proceed as follows. If the latter values are constrained by the future experiments, then we draw vertical gray lines in the top left panel such that the left vertical line intersects the lower future bound of NSI and the P2SO curve, while the right vertical line intersects the upper future bound of NSI and the P2SO curve. Therefore, for the values of $a_{e\mu}$ that lie outside the gray vertical lines, it is possible to have 3σ separation with $\epsilon_{e\mu}$, considering $\epsilon_{e\mu}$ is constrained by future experiments. Similar exercise can be done for the other parameters too. We have checked that conclusions obtained in these panels are consistent with Figs. 3 and 4 and therefore with Table V.

VII. SUMMARY

In this paper, we made an attempt to discriminate NSI and LIV in the context of the long-baseline experiments

DUNE and P2SO. Though the origin of the NSI and LIV theories are very different, they manifest themselves in a similar fashion in the Hamiltonian of the neutrino oscillation. The only difference is that the phenomenon of NSI depends on the earth matter density whereas LIV is independent of the matter density. Therefore, in the fixed baseline experiments where the matter density is constant, it is very difficult to distinguish NSI from LIV, as these effects become almost identical. However, as the present and future bounds of the NSI and LIV parameters are not equivalent, it is possible to separate these two theories with respect to their present/future bounds in the long-baseline experiments. Our choice of the experiments are motivated by the fact that DUNE and P2SO are the two long-baseline experiments that can have the most probable sensitivity to matter effect with the highest possible statistics.

In our work, we demonstrated the possibilities of discriminating LIV from NSI taking the present and future bounds of the NSI parameters. While compiling the bounds on the NSI and LIV parameters, we found that the future bounds of the NSI and LIV parameters are one order of magnitude better than the present available bounds except the parameters $\epsilon_{\mu\mu}$ and $a_{\mu\tau}$. At the probability level, we have seen that the separation between LIV and NSI is better when one considers the future bounds on the NSI parameters compared to their present bounds. Considering LIV in the data and NSI in theory, we find that indeed the capability of DUNE and P2SO to distinguish LIV from NSI improves when one considers the future bounds of the NSI parameters compared to present bounds. For the parameters ee and $\tau\tau$, it is impossible to separate LIV

from NSI for the current bounds of NSI parameters. The improvement in the sensitivity due to the future bounds on NSI is higher in the parameters that appear in the appearance channel, compared for the ones in the disappearance channel. Between the two experiments, the sensitivity of P2SO is better than DUNE except in the $e\mu$ sector. Our results show that the best discrimination between LIV and NSI is possible at 3σ C.L. for the parameter $a_{\mu\mu}$. In this case, the value of the LIV parameter falls inside its future bound if one considers the value of the NSI parameter to be constrained by the present experiments. The worst sensitivity comes from the sectors ee and $\tau\tau$. For these parameters, one cannot separate LIV from NSI if one considers the NSI parameters to be constrained by the present experiments.

To conclude, we find that the P2SO experiment is best suited to discriminate between the NSI and LIV scenarios and in particular, the new physics effects associated with the $\mu\mu$ sector.

[1] I. Esteban, M. C. Gonzalez-Garcia, M. Maltoni, T. Schwetz, and A. Zhou, The fate of hints: Updated global analysis of three-flavor neutrino oscillations, J. High Energy Phys. 09 (2020) 178.

[2] T. Ohlsson, Status of non-standard neutrino interactions, Rep. Prog. Phys. **76,** 044201 (2013).

[3] O. G. Miranda and H. Nunokawa, Non standard neutrino interactions: Current status and future prospects, New J. Phys. **17,** 095002 (2015).

[4] Y. Farzan and M. Tortola, Neutrino oscillations and nonstandard interactions, Front. Phys. **6,** 10 (2018).

[5] M. Mewes, Lorentz violation and neutrinos, in *3rd Meeting on CPT and Lorentz Symmetry*, pp. 29–37, 2005, arXiv:hep-ph/0409344.

[6] L. Wolfenstein, Neutrino oscillations in matter, Phys. Rev. D **17,** 2369 (1978).

[7] D. Colladay and V. A. Kostelecky, Lorentz violating extension of the standard model, Phys. Rev. D **58,** 116002 (1998).

[8] M. Masud, A. Chatterjee, and P. Mehta, Probing *CP* violation signal at DUNE in presence of non-standard neutrino interactions, J. Phys. G **43,** 095005 (2016).

[9] A. de Gouvêa and K. J. Kelly, Non-standard neutrino interactions at DUNE, Nucl. Phys. **B908,** 318 (2016).

[10] P. Coloma, Non-Standard Interactions in propagation at the deep underground neutrino experiment, J. High Energy Phys. 03 (2016) 016.

[11] J. Liao, D. Marfatia, and K. Whisnant, Degeneracies in long-baseline neutrino experiments from nonstandard interactions, Phys. Rev. D **93,** 093016 (2016).

[12] M. Masud and P. Mehta, Nonstandard interactions spoiling the *CP* violation sensitivity at DUNE and other long baseline experiments, Phys. Rev. D **94,** 013014 (2016).

[13] S. C and R. Mohanta, Implications of lepton flavor violation on long baseline neutrino oscillation experiments, Phys. Rev. D **94,** 053008 (2016).

[14] P. Coloma and T. Schwetz, Generalized mass ordering degeneracy in neutrino oscillation experiments, Phys. Rev. D **94,** 055005 (2016).

[15] M. Masud and P. Mehta, Nonstandard interactions and resolving the ordering of neutrino masses at DUNE and other long baseline experiments, Phys. Rev. D **94,** 053007 (2016).

[16] M. Blennow, S. Choubey, T. Ohlsson, D. Pramanik, and S. K. Raut, A combined study of source, detector and matter non-standard neutrino interactions at DUNE, J. High Energy Phys. 08 (2016) 090.

[17] S. K. Agarwalla, S. S. Chatterjee, and A. Palazzo, Degeneracy between θ_{23} octant and neutrino non-standard interactions at DUNE, Phys. Lett. B **762,** 64 (2016).

[18] M. Blennow, P. Coloma, E. Fernandez-Martinez, J. Hernandez-Garcia, and J. Lopez-Pavon, Non-unitarity, sterile neutrinos, and non-standard neutrino interactions, J. High Energy Phys. 04 (2017) 153.

[19] S. Fukasawa, M. Ghosh, and O. Yasuda, Sensitivity of the T2HKK experiment to nonstandard interactions, Phys. Rev. D **95,** 055005 (2017).

[20] K. N. Deepthi, S. Goswami, and N. Nath, Can nonstandard interactions jeopardize the hierarchy sensitivity of DUNE?, Phys. Rev. D **96,** 075023 (2017).

[21] J. Liao, D. Marfatia, and K. Whisnant, Nonstandard neutrino interactions at DUNE, T2HK, and T2HKK, J. High Energy Phys. 01 (2017) 071.

[22] M. Ghosh and O. Yasuda, Effect of systematics in the T2HK, T2HKK, and DUNE experiments, Phys. Rev. D **96,** 013001 (2017).

[23] M. Masud, M. Bishai, and P. Mehta, Extricating new physics scenarios at DUNE with higher energy beams, Sci. Rep. **9,** 352 (2019).

[24] M. Ghosh and O. Yasuda, Testing NSI suggested by solar neutrino tension in T2HKK and DUNE, Mod. Phys. Lett. A **35,** 2050142 (2020).

[25] K. N. Deepthi, S. Goswami, and N. Nath, Challenges posed by non-standard neutrino interactions in the determination of δ_{CP} at DUNE, Nucl. Phys. **B936,** 91 (2018).

[26] D. Meloni, On the systematic uncertainties in DUNE and their role in new physics studies, J. High Energy Phys. 08 (2018) 028.

[27] L. J. Flores, E. A. Garcés, and O. G. Miranda, Exploring NSI degeneracies in long-baseline experiments, Phys. Rev. D **98,** 035030 (2018).

[28] S. Verma and S. Bhardwaj, Nonstandard interactions and prospects for studying standard parameter degeneracies in DUNE and T2HKK, Adv. High Energy Phys. **2019,** 8464535 (2019).

[29] M. Masud, S. Roy, and P. Mehta, Correlations and degeneracies among the NSI parameters with tunable beams at DUNE, Phys. Rev. D **99,** 115032 (2019).

[30] J. Liao, N. Nath, T. Wang, and Y.-L. Zhou, Nonstandard neutrino interactions and mu-tau reflection symmetry, Phys. Rev. D **101,** 095036 (2020).

[31] B. Abi *et al.* (DUNE Collaboration), Prospects for beyond the standard model physics searches at the deep underground neutrino experiment, Eur. Phys. J. C **81,** 322 (2021).

[32] P. Bakhti and M. Rajaee, Sensitivities of future reactor and long-baseline neutrino experiments to NSI, Phys. Rev. D **103,** 075003 (2021).

[33] S. S. Chatterjee, P. S. B. Dev, and P. A. N. Machado, Impact of improved energy resolution on DUNE sensitivity to neutrino non-standard interactions, J. High Energy Phys. 08 (2021) 163.

[34] W.-J. Feng, J. Tang, T.-C. Wang, and Y.-X. Zhou, Nonstandard interactions versus planet-scale neutrino oscillations, Phys. Rev. D **100,** 115034 (2019).

[35] D. K. Singha, M. Ghosh, R. Majhi, and R. Mohanta, Optimal configuration of Protvino to ORCA experiment for hierarchy and non-standard interactions, J. High Energy Phys. 05 (2022) 117.

[36] S. K. Agarwalla, S. Das, M. Masud, and P. Swain, Evolution of neutrino mass-mixing parameters in matter with non-standard interactions, J. High Energy Phys. 11 (2021) 094.

[37] A. Khatun, S. S. Chatterjee, T. Thakore, and S. Kumar Agarwalla, Enhancing sensitivity to non-standard neutrino interactions at INO combining muon and hadron information, Eur. Phys. J. C **80,** 533 (2020).

[38] A. Kumar, A. Khatun, S. K. Agarwalla, and A. Dighe, A new approach to probe non-standard interactions in atmospheric neutrino experiments, J. High Energy Phys. 04 (2021) 159.

[39] J. Barranco, A. Bolanos, E. A. Garces, O. G. Miranda, and T. I. Rashba, Tensorial NSI and Unparticle physics in neutrino scattering, Int. J. Mod. Phys. A **27,** 1250147 (2012).

[40] J. Barranco, O. G. Miranda, C. A. Moura, and J. W. F. Valle, Constraining non-standard neutrino-electron interactions, Phys. Rev. D **77,** 093014 (2008).

[41] C. Biggio, M. Blennow, and E. Fernandez-Martinez, General bounds on non-standard neutrino interactions, J. High Energy Phys. 08 (2009) 090.

[42] M. C. Gonzalez-Garcia and M. Maltoni, Determination of matter potential from global analysis of neutrino oscillation data, J. High Energy Phys. 09 (2013) 152.

[43] M. C. Gonzalez-Garcia, Y. Grossman, A. Gusso, and Y. Nir, New *CP* violation in neutrino oscillations, Phys. Rev. D **64,** 096006 (2001).

[44] G. Barenboim, M. Masud, C. A. Ternes, and M. Tórtola, Exploring the intrinsic Lorentz-violating parameters at DUNE, Phys. Lett. B **788,** 308 (2019).

[45] S. Kumar Agarwalla and M. Masud, Can Lorentz invariance violation affect the sensitivity of deep underground neutrino experiment?, Eur. Phys. J. C **80,** 716 (2020).

[46] N. Fiza, N. R. Khan Chowdhury, and M. Masud, Investigating Lorentz violation with the long baseline experiment P2O, J. High Energy Phys. 01 (2023) 076.

[47] S. Sahoo, A. Kumar, and S. K. Agarwalla, Probing Lorentz invariance violation with atmospheric neutrinos at INO-ICAL, J. High Energy Phys. 03 (2022) 050.

[48] K. Abe *et al.* (Super-Kamiokande Collaboration), Test of Lorentz invariance with atmospheric neutrinos, Phys. Rev. D **91,** 052003 (2015).

[49] M. G. Aartsen *et al.* (IceCube Collaboration), Neutrino interferometry for high-precision tests of Lorentz symmetry with IceCube, Nat. Phys. **14,** 961 (2018).

[50] R. Majhi, S. Chembra, and R. Mohanta, Exploring the effect of Lorentz invariance violation with the currently running long-baseline experiments, Eur. Phys. J. C **80,** 364 (2020).

[51] H.-X. Lin, J. Tang, S. Vihonen, and P. Pasquini, Nonminimal Lorentz invariance violation in light of the muon

anomalous magnetic moment and long-baseline neutrino oscillation data, Phys. Rev. D **105,** 096029 (2022).

[52] U. Rahaman, Looking for Lorentz invariance violation (LIV) in the latest long baseline accelerator neutrino oscillation data, Eur. Phys. J. C **81,** 792 (2021).

[53] A. Crivellin, F. Kirk, and M. Schreck, Implications of $SU(2)_L$ gauge invariance for constraints on Lorentz violation, J. High Energy Phys. 04 (2021) 082.

[54] P. Adamson *et al.* (MINOS Collaboration), A Search for Lorentz Invariance and *CPT* Violation with the MINOS Far Detector, Phys. Rev. Lett. **105,** 151601 (2010).

[55] S. R. Coleman and S. L. Glashow, High-energy tests of Lorentz invariance, Phys. Rev. D **59,** 116008 (1999).

[56] L. H. C. Borges and A. F. Ferrari, External sources in a minimal and nonminimal *CPT*-odd Lorentz violating Maxwell electrodynamics, Mod. Phys. Lett. A **37,** 2250021 (2022).

[57] C. A. Moura and F. Rossi-Torres, Searches for violation of *CPT* symmetry and Lorentz invariance with astrophysical neutrinos, Universe **8,** 42 (2022).

[58] P. Abreu *et al.* (Pierre Auger Collaboration), Testing effects of Lorentz invariance violation in the propagation of astroparticles with the Pierre Auger Observatory, J. Cosmol. Astropart. Phys. 01 (2022) 023.

[59] S. Sahoo, A. Kumar, S. K. Agarwalla, and A. Dighe, Core-passing atmospheric neutrinos: A unique probe to discriminate between Lorentz violation and non-standard interactions, arXiv:2205.05134.

[60] B. Abi *et al.* (DUNE Collaboration), Deep underground neutrino experiment (DUNE), far detector technical design report, Volume II: DUNE physics, arXiv:2002.03005.

[61] A. V. Akindinov *et al.*, Letter of interest for a neutrino beam from protvino to KM3NeT/ORCA, Eur. Phys. J. C **79,** 758 (2019).

[62] S. Adrian-Martinez *et al.* (KM3Net Collaboration), Letter of intent for KM3NeT 2.0, J. Phys. G **43,** 084001 (2016).

[63] V. A. Kostelecky and M. Mewes, Lorentz and CPT violation in neutrinos, Phys. Rev. D **69,** 016005 (2004).

[64] A. Kostelecky and M. Mewes, Neutrinos with Lorentz-violating operators of arbitrary dimension, Phys. Rev. D **85,** 096005 (2012).

[65] P. Huber, M. Lindner, and W. Winter, Simulation of long-baseline neutrino oscillation experiments with GLoBES (General Long Baseline Experiment Simulator), Comput. Phys. Commun. **167,** 195 (2005).

[66] P. Huber, J. Kopp, M. Lindner, M. Rolinec, and W. Winter, New features in the simulation of neutrino oscillation experiments with GLoBES 3.0: General Long Baseline Experiment Simulator, Comput. Phys. Commun. **177,** 432 (2007).

[67] J. Kopp, Efficient numerical diagonalization of hermitian 3×3 matrices, Int. J. Mod. Phys. C **19,** 523 (2008).

[68] D. K. Singha, M. Ghosh, R. Majhi, and R. Mohanta, Study of light sterile neutrino at the long-baseline experiment options at KM3NeT, arXiv:2211.01816.

[69] B. Abi *et al.* (DUNE Collaboration), Experiment simulation configurations approximating DUNE TDR, arXiv:2103.04797.

[70] G. L. Fogli, E. Lisi, A. Marrone, D. Montanino, and A. Palazzo, Getting the most from the statistical analysis of solar neutrino oscillations, Phys. Rev. D **66,** 053010 (2002).

[71] P. Huber, M. Lindner, and W. Winter, Superbeams versus neutrino factories, Nucl. Phys. **B645,** 3 (2002).

[72] S. Davidson, C. Pena-Garay, N. Rius, and A. Santamaria, Present and future bounds on nonstandard neutrino interactions, J. High Energy Phys. 03 (2003) 011.

[73] P. S. Bhupal Dev *et al.*, Neutrino non-standard interactions: A status report, SciPost Phys. Proc. **2,** 001 (2019).

[74] G. Mitsuka *et al.* (Super-Kamiokande Collaboration), Study of non-standard neutrino interactions with atmospheric neutrino data in Super-Kamiokande I and II, Phys. Rev. D **84,** 113008 (2011).

[75] S. Choubey and T. Ohlsson, Bounds on non-standard neutrino interactions using PINGU, Phys. Lett. B **739,** 357 (2014).

[76] J. Kopp, M. Lindner, T. Ota, and J. Sato, Non-standard neutrino interactions in reactor and superbeam experiments, Phys. Rev. D **77,** 013007 (2008).

[77] O. Yasuda, On the exact formula for neutrino oscillation probability by Kimura, Takamura and Yokomakura, arXiv:0704.1531.

[78] M. Masud and P. Mehta, Nonstandard interactions and resolving the ordering of neutrino masses at DUNE and other long baseline experiments, Phys. Rev. D **94,** 053007 (2016).

[79] U. K. Dey, N. Nath, and S. Sadhukhan, Non-standard neutrino interactions in a modified ν2HDM, Phys. Rev. D **98,** 055004 (2018).

[80] A. Chatterjee, F. Kamiya, C. A. Moura, and J. Yu, Impact of matter density profile shape on non-standard interactions at DUNE, arXiv:1809.09313.

[81] M. Esteves Chaves, D. Rossi Gratieri, and O. L. G. Peres, Improvements on perturbative oscillation formulas including non-standard neutrino Interactions, J. Phys. G **48,** 015001 (2020).